Design of the ALPS II Optical System

M. Diaz Ortiz[a], J. Gleason[a], H. Grote[b], A. Hallal[a], M. T. Hartman[c], H. Hollis[a], K.-S. Isleif[c], A. James[b], K. Karan[d], T. Kozlowski[a], A. Lindner[c], G. Messineo[a], G. Mueller[a], J. H. Põld[d], R. C. G. Smith[c], A. D. Spector[c,*], D. B. Tanner[a], L.-W. Wei[c], B. Willke[d]

[a] *Department of Physics, University of Florida, 32611 Gainesville, Florida, USA*
[b] *School of Physics and Astronomy, Cardiff University, CF24 3AA Cardiff, Wales, UK*
[c] *Deutsches Elektronen-Synchrotron DESY, Notkestr. 85, 22607 Hamburg, Germany*
[d] *Max-Planck-Institut für Gravitationsphysik (Albert-Einstein-Institut) and Leibniz Universität Hannover, 30167 Hannover, Germany*

Abstract

The Any Light Particle Search II (ALPS II) is an experiment currently being built at DESY in Hamburg, Germany, that will use a light-shining-through-a-wall (LSW) approach to search for axion-like particles. ALPS II represents a significant step forward for these types of experiments as it will use 24 superconducting dipole magnets, along with dual, high-finesse, 122 m long optical cavities. This paper gives the first comprehensive recipe for the realization of the idea, proposed over 30 years ago, to use optical cavities before and after the wall to increase the power of the regenerated photon signal. The experiment is designed to achieve a sensitivity to the coupling between axion-like particles and photons down to $g_{\alpha\gamma\gamma} = 2 \times 10^{-11}\mathrm{GeV}^{-1}$ for masses below 0.1 meV, more than three orders of magnitude beyond the sensitivity of previous laboratory experiments. The layout and main components that define ALPS II are discussed along with plans for reaching design sensitivity. An accompanying paper (Hallal, et al [1]) offers a more in-depth description of the heterodyne detection scheme, the first of two independent detection systems that will be implemented in ALPS II.

Keywords: axion search, laser interferometry, optical cavities, light-shining-through-a-wall
2010 MSC: 00-01, 99-00

1. Introduction

While the standard model has been extremely successful, a variety of phenomena suggest that it is still an incomplete description of our universe. One example of this is known as the strong CP problem in quantum chromodynamics (QCD), in which a term in the QCD Lagrangian will break CP symmetry if one of it constituent variables has a non zero value [2]. While, as an angle,

*Corresponding author
Email address: aaron.spector@desy.de (A. D. Spector)

it appears that this variable should be of order unity, no violations of CP symmetry in the strong force have ever been measured [3].

The solution proposed by Peccei and Quinn was to promote this variable to a dynamic field associated with a new elementary particle called the axion. This pseudo-Goldstone boson is characterized by the energy scale of the Peccei-Quinn symmetry breaking: the axion mass as well as its coupling strengths to standard model particles is inversely proportional to this energy scale. Experimental results indicate that the energy scale is far beyond the reach of particle accelerators resulting in very light-weight and very weakly coupled axions. These axions would also couple to photons via the following term in the Lagrangian [2, 4, 5]:

$$\mathcal{L}_a = g_{a\gamma\gamma}\phi_a \vec{E} \cdot \vec{B} \tag{1}$$

Here $g_{a\gamma\gamma}$ is the axion-photon coupling strength, ϕ_a is the axion field, the oscillating electric field is given by $\vec{E}$, and $\vec{B}$ represents a static magnetic field.

As it happens, axions could be the cause of a number of other phenomena that the standard model also fails to explain. While the most prominent example of this is the existence of cold dark matter [33], other anomalies such as stellar cooling rates that exceed predictions may also be explained by axions [28]. Furthermore, 'axion-like' particles which are not themselves the QCD axion, but share similar characteristics to it could explain other anomalous observations such as the transparency of the universe to TeV photons [27]. All of these hints are shown as the red regions in the axion-like particle parameter space in Figure 1.

One of the most promising strategies for axion searches involves the Sikivie effect, where in the presence of an external magnetic field, an axion will generate a photon [34]. There are a number of experiments that try to use this effect to observe axion-like particles and their designs are largely dependent on their respective sources of axions. Haloscopes such as ADMX and MADMAX look for axions that reside in the dark matter halo using microwave resonators immersed in a magnetic field [12, 35]. Helioscopes such as CAST and IAXO use the sun as a source of ultra-relativistic axions that then are converted to photons in a magnetic field and detected with X-ray telescopes placed at the end of the magnet [6, 36]. In contrast to these searches, light-shining-through-a-wall (LSW) experiments take place entirely in the laboratory using a high-power laser (HPL) propagating through a magnetic field. This generates a beam of axion-like particles that travel through a light-tight wall into a second magnetic field region where some of these axion-like particles convert back to photons [37]. The current limits on the axion-photon coupling from these different types of searches are shown as the solid blue regions in Figure 1, while limits from astronomical observations are shown as the solid green regions.

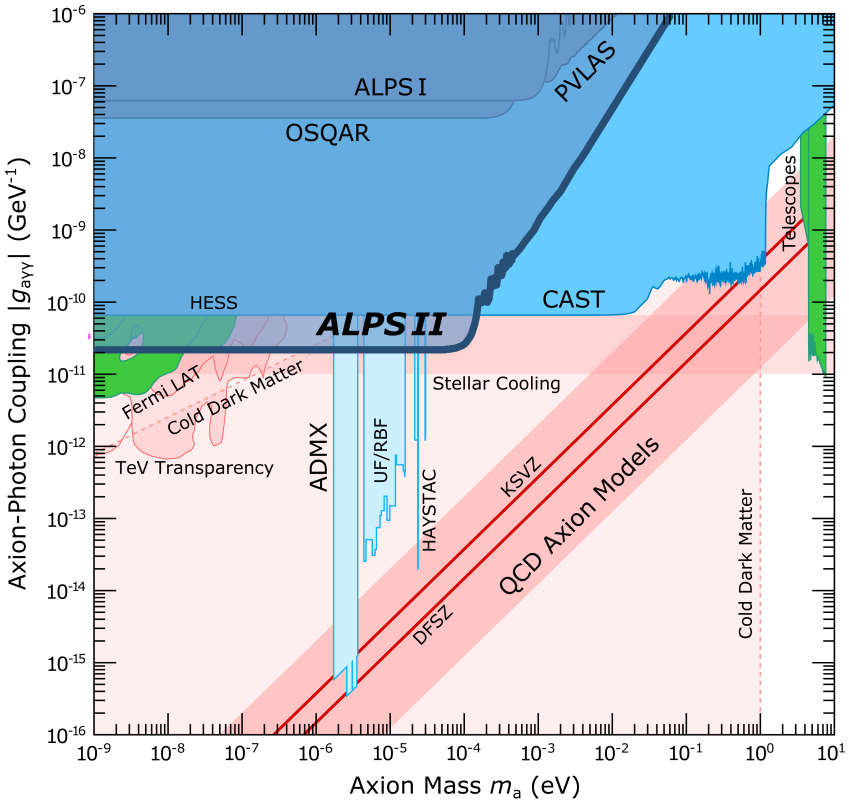

Figure 1: ALPS II target sensitivity, shown in the transparent blue region, along with current exclusion limits for axion-like-particles given in blue for the helioscopes [6], dark blue for the LSW experiments [7, 8, 9], light blue for dark matter haloscopes [10, 11, 12, 13, 14, 15, 16, 17, 18], and green for the astronomical observations [19, 20, 21]. Regions of the parameter space which offer hints of their existence are shown in red [22, 23, 24, 25, 26, 27, 28, 29, 30, 31, 32]. Please note that several exclusion limits rely on mostly untested assumptions such as axions or axion-like particles making up 100% of the dark matter in the milky way, structures of galactic and intergalactic magnetic fields, or axion and axion-like particles production in dense stellar plasmas.

It is worth emphasizing that LSW experiments make no assumptions regarding the natural prevalence of any of these particles, but merely probe the interactions themselves without the need for an external source. These experiments can therefore determine the photon-coupling strength independent of any astrophysical models, while solar searches and haloscopes, not only depend on the coupling strength, but also rely on models of the axion-flux.

The Any Light Particle Search II (ALPS II) [38] is a LSW experiment currently under construction at DESY in Hamburg, Germany. With DESY as the host site, the experiment takes advantage of the tunnels, magnets, and cryogenic infrastructure formerly used by the HERA accelerator. It will use 122 m long optical cavities to amplify light at a wavelength of 1064 nm that is generated on one side of the wall by a high-power laser (HPL) and by the photon regeneration process on the

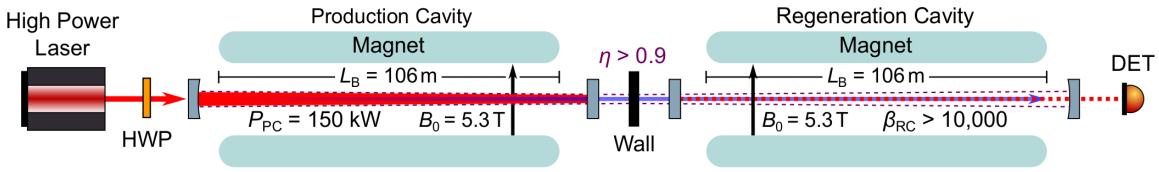

Figure 2: Experimental layout of ALPS II. The circulating fields in each cavity propagate through 560 T · m of the magnetic field times length product, with its length shown as L_B and the field strength given by B_0. The power inside the PC, shown as solid red, will be at least 150 kW, while the resonant enhancement of the RC β_{RC}, must be greater than 10,000. The coupling efficiency between the PC and RC, given by η, will be at least 0.9, with the projected spatial mode of the PC shown as the dotted purple line. A wall between the cavities prevents any light from the PC from directly entering the RC while a half wave plate (HWP) after the high power laser enables the polarization of the laser to be controlled with respect to the magnetic field. The axion like particle beam is seen as the blue line with the regenerated photon signal represented by the dotted red line that is incident on the detector at the right side of the diagram.

other side. The experiment is designed to increase the photon regeneration rate by twelve orders of magnitude over earlier LSW experiments [39, 40, 41, 42]. Like all LSW experiments, ALPS II will not only probe the existence of pseudo-scalar fields whose coupling to electromagnetic fields is described by Equation 1, but also scalar fields whose coupling can be described by the Lagrangian:

$$\mathcal{L}_s = g_{a\gamma\gamma}\phi_s(\vec{E}^2 - \vec{B}^2). \tag{2}$$

Experimentally, while the pseudo-scalar fields from Equation 1 require the polarization of the E-field and the B-field to be parallel, scalar fields require that the polarization of the E-field is orthogonal to the B-field. A signal running in both polarization modes with no observed polarization dependence on the production rate could be detected as well. This may indicate the existence of other types of Weakly Interacting Sub-eV Particles (WISPs) that are produced by kinetic mixing such as millicharged particles or hidden sector photons which do not require a static magnetic field to interact with photons [43]. In the following, we refer to particles whose interaction strength depends on $\vec{B}$ as axion-like particles, however the observation of any such particle would represent a profound discovery as it would be the first detection of an interaction beyond the standard model.

With a target sensitivity of $2 \times 10^{-11}\,\mathrm{GeV}^{-1}$, ALPS II aims to go beyond the current CAST limits by a factor of ∼3 for masses below 0.1 meV, investigating a new region of the axion-like particle parameter space that is occupied by hints from both stellar cooling excesses and the TeV transparency. In addition to this, ALPS II will also be the first model independent search in a significant region of the parameter space explored by CAST.

To achieve this, the entire optical setup including the two cavities must be tightly controlled to maintain and accurately calibrate the coupling of the generated axion field to the cavities. The

Table 1: Top level requirements for the first ALPS II science run targeting a sensitivity of $g_{\alpha\gamma\gamma} = 2.8 \times 10^{-11}\,\mathrm{GeV}^{-1}$ (adapted from [44]).

	Requirement
TLR1	$> 150\,\mathrm{kW}$ power circulating in PC (fundamental mode, linearly polarized, 1064 nm)
TLR2	Parallel and perpendicular polarization adjustment possibility with respect to the magnetic field
TLR3	Coupling between the axion mode and the RC fundamental mode: $\eta > 90\%$ (power ratio)
TLR4	RC resonant enhancement $\beta_{\mathrm{RC}} > 10\,000$
TLR5	Detector sensitive enough to exclude a reconverted photon rate $> 2.8 \times 10^{-5}$/s with a 95% confidence level within 20 days
TLR6	Magnetic field $\times$ length product of 560 T·m for PC and RC magnet string

following text will focus primarily on the core components that define the optical system for the experiment and discuss how we plan to reach the targeted sensitivity, while also providing a set of top level requirements for the subsystems. A complementary paper [1], builds on the work presented here and describes the heterodyne detection scheme (HET) in more detail.

1.1. ALPS II

As mentioned earlier, the optical system for ALPS II will consist of two 122 m long, high-finesse optical cavities whose circulating fields will propagate through strings of 12 superconducting HERA dipole magnets [45], as shown in Figure 2. A current of 5.7 kA will flow through the 8.8 m long dipoles and produce a magnetic field of 5.3 T giving a product of the magnetic field and length of $B_0 L = 560\,\mathrm{T{\cdot}m}$ on each side of the wall. On the left side of the wall, light with a wavelength of 1064 nm from the HPL will be resonant with the production cavity (PC), building up the stored energy due to the high cavity finesse. This light will generate axion-like particles, shown as the transparent blue line in Figure 2, with an identical energy and spatial mode, outlined by the purple dotted line. These particles pass through the light-tight barrier on the central optical bench (COB) before they enter the regeneration cavity (RC) where they convert back to photons, shown as the dotted red

line. The regenerated photon rate,

$$n_{\mathrm{reg}} = \frac{\eta}{16} \left(g_{a\gamma\gamma} F(qL_{\mathrm{B}}) B_0 L_{\mathrm{B}}\right)^4 \frac{P_{\mathrm{PC}}}{h\nu} \beta_{\mathrm{RC}}, \tag{3}$$

scales with $\left(g_{a\gamma\gamma} B_0 L\right)^4$ and is proportional to the power inside the PC in terms of photons per second, $P_{\mathrm{PC}}/h\nu$, and the resonant enhancement β_{RC} of the RC [46]. The form factor can be approximated by the following equation with L_{B} representing the 106 m length of each magnet string.

$$|F(qL_{\mathrm{B}})| \approx \left| \frac{2}{qL_{\mathrm{B}}} \sin\left(\frac{qL_{\mathrm{B}}}{2}\right) \right| \qquad \left(q = \frac{m_a^2}{2h\nu}\right) \tag{4}$$

This is a typical phase matching condition which accounts for the possible mass m_a, of the relativisitic axion-like particles. For masses $m_a < 0.1\,\mathrm{meV}$, the form factor is essentially unity in ALPS II. For a more detailed discussion on this please see [46].

The coupling efficiency η between the relativistic axion field and the eigenmode of the RC takes into account all transversal and spectral mismatches between the axion mode, which is identical to the PC eigenmode, and the eigenmode of the RC. Here η is given in terms of axion to photon coupling and therefore the axion field to electromagnetic field coupling would be given by $\sqrt{\eta}$. It will be possible to verify η before and after measurement runs by opening a shutter in the light tight barrier and allowing the PC transmitted field to couple to RC.

Table 1 lists the top level requirements (TLR) of ALPS II. While the long magnet string (TLR 6) provides a sensitivity gain of ~ 25 in $g_{a\gamma\gamma}$ when compared to ALPS I, TLR 1, requiring a PC internal power of 150 kW, and TLR 4, requiring an RC resonant enhancement $\beta_{\mathrm{RC}} > 10\,000$, together increase the sensitivity of the experiment by a factor of ~ 40, demonstrating the importance of the optical system. Achieving both of these requirements depends on the coatings and surface roughnesses of the cavity mirrors as well as clipping losses in the magnet strings. This will be discussed further in section 2. It should be noted TLR 4 is not far from the limits of what is possible for mirrors of these dimensions with state of the art polishing techniques. TLR 3 refers to the coupling of the axion field to the RC and is discussed in section 3. TLR 5 not only establishes requirements on the sensitivity of the detection systems, but can also be used to set the maximum permissible background signal due to stray light coupling from the PC to the detectors.

The first science run will be a search based on the above listed parameters that could set an upper limit of $g_{\alpha\gamma\gamma} = 2.8 \times 10^{-11}/\mathrm{GeV}$ corresponding to an upper limit on the regenerated photon rate of $2.8 \times 10^{-5}/\mathrm{s}$ or roughly 2.4 photons per 24 h of valid data. This search will be followed by a scalar particle search at the same sensitivity by changing the polarization (TLR 2). We will then attempt to improve the sensitivity by increasing the PC circulating power, the RC resonant

enhancement, and the duty cycle to aim for $g_{\alpha\gamma\gamma} = 2 \times 10^{-11}$/GeV or better [44] for pseudo-scalar and scalar particles.

1.2. Detection Systems

ALPS II will have the benefit of using two independent detection systems, each with very different systematic uncertainties, to measure the reconverted photons. While two different detector types are not explicitly needed, this approach will help increase confidence that signals observed with the same strength in both detectors, while also above the measured backgrounds, are indeed the result of photon-axion conversion-reconversion process. The detectors themselves require different optical systems in order to be operated and therefore cannot be used in parallel. Working at a wavelength of 1064 nm implies that free-space, off-the-shelf, silicon photodetectors have plenty of sensitivity to be used as detectors in the control system and also for the ALPS II heterodyne readout. Only the single-photon counting approach requires more sensitive detectors, which are under development.

The first detection scheme to be implemented will be the HET, described in an accompanying paper in this journal [1]. The HET measures the interference beatnote between a laser, referred to as the local oscillator (LO), and the regenerated photon field on a photodetector. Demodulating the electronic signal from this photodetector at the known difference frequency will create a signal proportional to the regenerated field strength that can be integrated over the measurement time τ. The regenerated photon signal will thus accumulate proportional to τ while the background signal from laser shot noise will sum incoherently and thus be proportional to $\sqrt{\tau}$ [47].

A transition edge sensor (TES) will be used in the second detection system [48]. In contrast to the HET system based on interference effects, the TES system will count individual photons. The TES consists of an absorptive tungsten film which is held at a temperature at the threshold of superconductivity. When a photon is absorbed by the tungsten it will lead to a slight increase in its temperature. This will suddenly raise the resistance of the chip causing a drop in the bias current that is flowing through it. This current drop can be measured over an inductive coil with a superconducting quantum interference device. Therefore, the reconverted photons can be individually counted as these pulses occur, with an energy resolution of $\sim 7\%$. A laboratory prototype TES currently triggers at about 0.8 eV, but this is not necessarily the final configuration. Saturation occurs at energies well above 2.3 eV (wavelengths below 532 nm), and can be tuned with the TES working point. A forthcoming paper will offer more details about the TES detection system, including details of the involved optical fiber system as well as the interplay between the 1.17 eV energy of the reconverted photons and the TES system.

Table 2: Parameters of the ALPS II cavities

Parameter (symbol/acronym)	Value
Length ($L_{\mathrm{PC/RC}}$)	122 m
Free spectral range (FSR)	1.2 MHz
Half-width-half-maximum (HWHM)	15 ± 2.5 Hz
End mirror radius of curvature (R)	214 ± 6 m
$1/e^2$ waist radius (w_0)	6.0 mm
$1/e^2$ end mirror beam radius (w_{m})	9.2 mm
Divergence half angle (θ_{Div})	57 µrad
RC resonant enhancement (β)	$16\,000 \pm 2\,000$

2. ALPS II Cavities

Both the PC and RC will be plano-concave cavities with a stability parameter $g = 0.43$. The curved mirrors will be located at the end stations of the experiment while the flat mirrors will be at the center as shown in Figure 2. The radius of curvature of the mirrors at the end stations were chosen such that the Rayleigh lengths of the cavity eigenmodes, z_R, are equal to the length of their corresponding magnet strings. This geometry will help minimize aperture losses in the cavities while also avoiding higher order mode degeneracies that would occur if the cavities were exactly half-confocal. The configuration also ensures that the eigenmodes of both cavities can have a high spatial overlap as the nominally identical Gaussian beam waists are located on the flat mirrors. The distance between the flat cavity mirrors (< 1 m) is much smaller than the Rayleigh length (~ 106 m) of the modes rendering the resulting loss in coupling negligible compared to other contributions.

The cavity eigenmodes will need to be centered within the beam tube of the magnet string to reduce clipping losses. The diameter of the magnet aperture is nominally 55 mm, however since the magnets were originally used to steer protons around the arcs of the HERA accelerator, their central axis followed a curvature of 600 m and therefore required straightening. This process was very successful, and expanded the free apertures of the magnets from ∼37 mm to between 46 and 51 mm [45]. The largest free aperture magnets will be used near the end stations where the beam size and risk of clipping losses is the highest.

The magnets along with the rest of the vacuum system that will house the cavities are now aligned within ± 200 µm and ± 1 µrad of a line defining the theoretical optical axis of the experiment. The cavity mirrors will then be placed within ± 1 mm and ± 8 µrad of the resulting central line of the

combined magnet string, reducing clipping losses inside the two cavities to below 1 ppm.

2.1. Regeneration cavity

The resonant enhancement provided by the regeneration cavity:

$$\beta_{\mathrm{RC}} \approx \frac{4T_{\mathrm{out}}}{\left(T_{\mathrm{out}} + T_b + \rho\right)^2}, \tag{5}$$

is very similar to the power build-up ratio between the input power and the maximum circulating power for a generic optical cavity. In this case, it expresses the gain in signal power at the detector due to the amplification of the cavity. As Equation 5 shows, it depends on the losses and transmissivities of each mirror. Here T_{out} is the transmissivity of the mirror located nearest to the main regenerated photon detector while T_b is the transmissivity of the other cavity mirror. Ideally, the maximum resonant enhancement occurs when the RC has minimal round-trip losses ρ, and the mirror transmissivities are as low as possible and the cavity is in the so-called 'impedance matched' configuration where $T_{\mathrm{out}} = T_b + \rho$.

Losses in our cavities are expected to be dominated by the surface roughness of the mirrors and the associated scattering of light. Simulations using measured surface maps of the actual mirror substrates predict that the scatter losses inside the cavity will likely be between 40 and 60 ppm per round-trip. Operating the RC in an 'over-coupled configuration' ($T_{\mathrm{out}} > T_b + \rho$) will simplify the HET detection scheme as it will allow for a more stable power in the LO at the science photodetector [1]. Therefore, to be conservative, we decided to use 100 ppm as the design value for T_{out} for the initial science run. T_b will then be 5 ppm since the HET also requires some nonzero transmission for this mirror to realize the sensing and control scheme. This is discussed in more detail in Section 3.

The dielectric cavity mirror coatings consist of alternating $\lambda/4$ layers of silica and tantala to minimize the absorptive losses; note that the same coatings will also be used in the PC where laser beam absorption will lead to thermal distortions of the cavity eigenmode. These mirrors were received and measured to have transmissivities of ~ 110 ppm and ~ 6.7 ppm at normal incidence which results in an expected resonant enhancement of

$$\beta_{\mathrm{RC}} \approx 16\,000 \pm 2\,000 \tag{6}$$

given the expected scattering losses and their corresponding uncertainty.

2.2. Production cavity

The PC will be seeded with the HPL, a linear polarized laser beam from a single-frequency, low-noise laser system operating at 1064 nm capable of injecting up to 50 W to the cavity. The HPL is based on a master-oscillator power-amplifier configuration (MOPA) with an ultra stable Nd:YAG

seed laser in non-planar ring-oscillator configuration [49] and a low-noise Nd:YVO_4 amplifier [50] with a high spatial purity. The challenge for the laser design is to generate a high power beam with small fluctuations and drifts that allows for a highly efficient coupling of the light into the PC. In this regard the chosen MOPA design is advantageous as it preserves the high frequency stability of the seed laser and has, compared to an oscillator, relatively low intensity levels in the gain material such that thermally induced wave front distortions and depolarization effects can be minimized.

Light from the HPL will then be incident on the PC. The PC will use mirrors with identical dielectric coatings as the RC mirrors. Therefore, the PC power build-up factor is also expected to be $16\,000 \pm 2\,000$, the same as the resonant enhancement of the RC. A frequency stabilization system with a unity gain frequency of $\sim 300\,\mathrm{kHz}$ will maintain the resonance of the laser with respect to the length of the PC using the standard Pound-Drever-Hall (PDH) technique [51, 52]. The sensing scheme and the loop gain are expected to keep the laser frequency within a hundredth of the half-width-half-maximum (HWHM) of the cavity resonance corresponding to a relative power noise inside the cavity to a RMS value $<100\,\mathrm{ppm}$.

The input optics between the high-power laser (HPL) and the PC will also be equipped with an automatic alignment system based on a differential wavefront sensing (DWS) scheme. This system uses a pair of quadrant photodetectors (QPDs) which measure the lateral shift and angular offset between the laser mode and the cavity eigenmode [53]. These signals are then fed back to a pair of actuators to maintain the alignment of the laser into the cavity. The goal is to also limit the RMS relative power noise inside the cavity due to alignment fluctuations to $<100\,\mathrm{ppm}$ for each degree of freedom. The entire system will guarantee that the total relative power noise stays below 0.1% RMS, which should be sufficient to reduce the impact of dynamic thermal effects on the HET [1]. The input optics for the PC will also employ a half-waveplate to rotate the polarization of the circulating field with respect to the polarity of the magnet string. This will satisfy TLR2 and allow the experiment to search for either scalar or pseudo-scalar particles.

This combination of the HPL and cavity finesse may allow powers as high as 1 MW inside the PC, however, the final power level will likely be limited by the absorption in the highly-reflective coating layers of the two cavity mirrors. There are a number of ways this absorbed light could lead to thermal effects that cause higher intracavity losses. For example, point absorbers heating up on the surface of the mirror could cause the formation of low spatial frequency features which, in turn, leads to an increase in the scattering losses [54, 55]. Absorption in the mirror coatings could also cause the size of the mode circulating in the PC to change and lead to additional clipping loses from the beam tube [56]. The loss in sensitivity due to the mode mismatch between the cavity eigenmodes as the PC mirrors heat up is expected to be insignificant in comparison. Nevertheless, 150 kW with

Table 3: Requirements for fulfilling TLR3

Parameter (symbol)	Requirement
Axion coupling to RC (η)	>90%
Coherence $(\eta_{\Delta f})$	>95%
dynamic phase noise $(\Delta\phi_{\mathrm{SD}})$	<0.2 rad
static frequency offset (Δf)	<1.5 Hz
Spatial overlap (η_{T})	>95%
Angular alignment $(\Delta\theta)$	<5.7 µrad
Transversal shift (Δx)	<1.2 mm

the beam size on the PC mirror is roughly equivalent to the peak circulating intensity in the aLIGO pre-mode cleaner and is therefore expected to be attainable [57].

3. Maintaining the Axion Field Coupling to the RC

The primary obstacles to optimizing the coupling of the axion field to the RC are related to maintaining its coherence and spatial mode matching with respect to the RC eigenmode. These parameters will depend on the residual changes of the frequency and spatial mode of the PC circulating field with respect to the RC. As Table 3 shows, we allow each to contribute a 5% loss of the signal to meet the 90% coupling efficiency listed under TLR 3. Here we can also see that each of these requirements can be further subdivided into requirements on specific parameters of the optical system. The following sections discuss how each of these requirements are derived and how the optical system will work to satisfy them.

3.1. Coherence of the PC field with the RC

Maintaining the coherence between the electromagnetic field regenerated from the axion beam and the RC eigenmode is critical to ALPS II achieving its target sensitivity. Therefore, the optical system is designed such that the regenerated field should experience no more than 5% average reduction from its optimal resonant enhancement over the duration of the measurement due to its frequency noise with respect to the RC resonance frequency. This requirement is further divided into one on static frequency offset, denoted by Δf, and one on the dynamic phase noise, denoted by $\Delta\phi_{\mathrm{SD}}$. As the regenerated field is a replica of the field circulating in the PC, the first challenge is to accurately tune the frequency of the PC transmitted field to be resonant with the RC. The second challenge is to precisely control the phase of the PC transmitted field around this nominal value.

3.1.1. PC Tuning

The signal loss in regenerated photons due to a small offset of Δf in the frequency of the PC transmitted light relative to a resonance frequency of the RC is quadratic in the offset and can be approximated by the following expression.

$$1 - \eta_{\Delta f} \approx \left(\frac{\Delta f}{\mathrm{HWHM}}\right)^2 \tag{7}$$

Here HWHM is the half-width half-max linewidth of the RC. To limit the loss of regenerated photons to 1%, we require that the detuning is less than 10% of the HWHM or less than 1.5 Hz during the science run.

As Figures 3 shows, the optical system when using the HET will control the frequency of the PC transmitted field, ν_{PC}, via a series of offset phase lock loops (PLLs). This will allow ν_{PC} to track the changes in the resonance frequency of the RC due to the presence of environmental noise. To do this the LO is stabilized to the length of the RC with a high bandwidth control loop (>300 kHz) ensuring that the frequency of the transmitted LO field is equivalent to the RC resonance ν_{RC}. The phase of the transmitted LO field, ϕ_{RC}, will therefore be encoded with the RC length noise. An auxiliary laser, referred to as the reference laser (RL), will then be phase locked to ν_{RC} with some offset f_0 giving it a frequency $\nu_{\mathrm{RL}} = \nu_{\mathrm{RC}} + f_0$. By setting $f_0 \neq FSR_{\mathrm{RC}}$, the RL will not be resonant in the RC. Finally, since the HPL is frequency stabilized to the length of the PC, an offset phase lock loop between RL and the PC transmitted field will be established to suppress the dynamic phase noise $\delta\phi_{\mathrm{PC}} - \delta\phi_{\mathrm{RC}}$ (as discussed in Section 3.1.2). This gives ν_{PC} the following value with any unintended offsets expressed as Δf:

$$\nu_{\mathrm{PC}} = \nu_{\mathrm{RL}} - f_0 + N \cdot FSR_{\mathrm{RC}} + \Delta f = \nu_{\mathrm{RC}} + N \cdot \mathrm{FSR}_{\mathrm{RC}} + \Delta f. \tag{8}$$

With Δf sufficiently small, the PC circulating field should be offset in frequency from ν_{RC} by some integer multiple of $\mathrm{FSR}_{\mathrm{RC}}$, N, thus making it resonant in the RC. Δf will be minimized tuning the

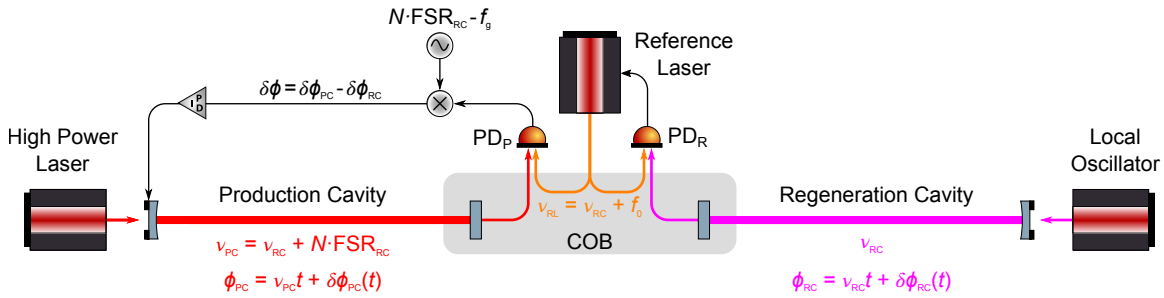

Figure 3: Layout of the cavities and control architecture for maintaining the phase lock of the PC in the HET optical system.

PLL offset frequencies to maximize the coupling of the PC transmitted field to the RC with the shutter open. During the science runs these values must be maintained when the shutter is closed [1]. This approach requires that the source for the offset frequency and the FSR of the RC are both stable.

The RL-LO beatnote frequency, f_0, will be derived from a clock that is synchronized to a 10 MHz rubidium frequency standard with a yearly frequency drift on the order of mHz, well below our requirement. However, macroscopic changes of the length of the RC will change the optimum offset frequency by:

$$\Delta f_{_{\Delta\mathrm{FSR}}} = N \cdot \Delta\mathrm{FSR}_{_{\mathrm{RC}}} = N \cdot \mathrm{FSR}_{_{\mathrm{RC}}} \frac{\Delta L_{_{\mathrm{RC}}}}{L_{_{\mathrm{RC}}}} \tag{9}$$

The length changes of the RC then have to be

$$\Delta L_{_{\mathrm{RC}}} < \frac{\Delta f_{_{\Delta\mathrm{FSR}}}}{\mathrm{FSR}_{_{\mathrm{RC}}}} \frac{L_{_{\mathrm{RC}}}}{N} = \frac{150\,\mu\mathrm{m}}{N} \tag{10}$$

between retuning measurements to ensure that $\Delta f < 1.5\,\mathrm{Hz}$. A FSR sensing system that uses a modified PDH sensing technique which uses phase modulated sidebands at some multiple ($\neq N$) of the FSR will also be implemented [58]. With this ΔL will be measured continuously during the science run and if it becomes larger than $150\,\mu\mathrm{m}/N$ the run will be paused and the length of the RC will be adjusted back to its initial value before it is started again. Options to actively control the length of the RC during measurement runs are also being evaluated.

3.1.2. Phase lock of the PC

The series of PLLs mentioned in the previous section will also be used to reduce the frequency or phase fluctuations $\delta\phi(t)$, of the PC transmitted field relative to the resonant frequency of the RC. This system must provide the precision necessary to meet the requirements on the coherence. Phase noise will spread the energy of the ideally monochromatic PC transmitted field over a finite frequency band and only the frequency components which are resonant in the RC will contribute to the signal. The energy in all frequency components outside the line-width of the RC will be attenuated.

We require that the power integrated over all frequency components outside this bandwidth is less than 4% of the total power. This requirement roughly translates into an upper limit for the standard deviation (SD) of the phase noise evaluated over the storage time $\mathcal{T}$ of the cavity of [59]:

$$\Delta\phi_{_{\mathrm{SD}}}(t) \approx \sqrt{\langle \delta\phi^2(t) \rangle_{\mathcal{T}}} < 0.2\,\mathrm{rad} \tag{11}$$

which the phase lock loop between the PC transmitted field and the reference field must achieve.

Due to the high gain and fast bandwidth ($\sim 300\,\mathrm{kHz}$) of the control loop that stabilizes the HPL to the PC, the phase of the PC transmitted light should be almost entirely determined by the PC

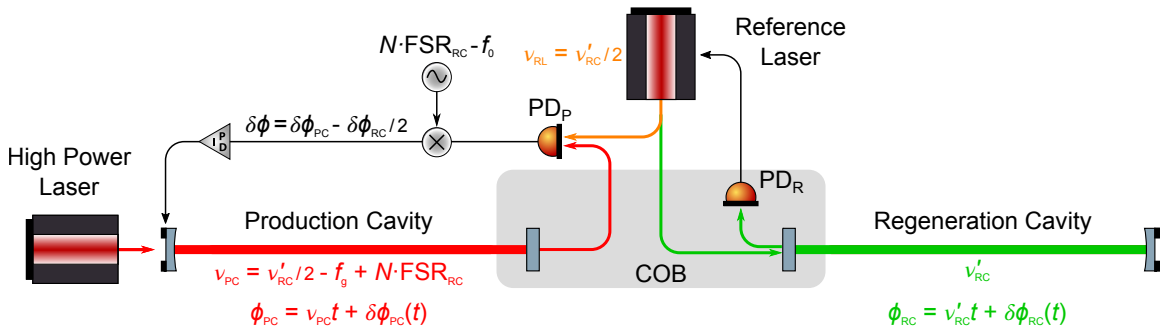

Figure 4: Layout of the cavities and control architecture for maintaining the phase lock of the PC in the TES optical system.

length. The PLL must then act on the length of the PC such that it follows all length changes of the RC which are impressed on the phase of the reference laser as shown in Figure 3.

For this purpose, we developed a piezo-electric actuated mirror mount for the 2" diameter PC input mirror that supports a control bandwidth of 4 kHz. Based on seismic measurements in the HERA tunnel, this bandwidth, paired with an aggressive gain function is expected to be sufficient to suppress the environmental noise [59].

3.1.3. Maintaining coherence with the TES optical system

The TES optical system is also designed to maintain the resonance of the PC circulating field with respect to the RC, but has slightly different constraints due to the nature of the detector. While the HET is capable of distinguishing fields with sub-Hz frequency differences [47], the presence of these signals at the detector would saturate the TES, in addition to creating backgrounds indistinguishable from the regenerated field. Therefore, the frequency of any field that may be incident on the TES must be different enough from ν_{PC} such that it can be sufficiently suppressed by optical filters and can also be distinguished from the signal field during data processing. For this reason the optical system for the TES will appear as seen in Figure 4. Here the RL is frequency doubled from 1064 nm to a wavelength of 532 nm and the laser is then frequency stabilized to the RC length with the green light coupled to the cavity. With this $\nu_{\mathrm{RL}} = \nu'_{\mathrm{RC}}/2$, where ν'_{RC} is the resonance frequency of the RC for 532 nm. This allows the green light to be filtered out of the path to the detector (not shown). Furthermore, the TES is capable of differentiating between photons with wavelengths of 532 nm and 1064 nm.

As is the case in the HET optical system, the PC transmitted field is then offset phase locked to the 1064 nm light from RL by actuating on the length of the PC. The frequency of the PC

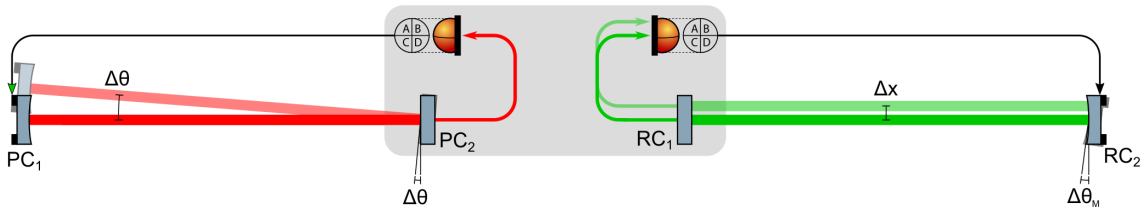

Figure 5: Control architecture for maintaining spatial overlap. The QPDs on the COB monitor the position of the cavity eigenmodes on the cavity mirrors PC_2 and RC_1. These signals are used to align the cavity mirrors at the end stations PC_1 and RC_2. The aligned configuration is shown as the solid image in the foreground, while examples of the potential alignment errors are shown as transparent images in the background.

transmitted field is therefore:

$$\nu_{\mathrm{PC}} = \nu_{\mathrm{RL}} - f_{\mathrm{g}} + N \cdot FSR_{\mathrm{RC}} = \frac{\nu'_{\mathrm{RC}}}{2} - f_{\mathrm{g}} + N \cdot FSR_{\mathrm{RC}} \tag{12}$$

In this equation f_{g} accounts for the relative frequency offset between the green and IR resonances due to the difference in the reflected phase between the two wavelengths. To ensure that the PC circulating field is resonant in the RC, the beatnote frequency, $\nu_{\mathrm{PC}} - \nu_{\mathrm{RL}}$, must be tuned for either an even or odd number integer multiple of green wavelengths in the RC because of f_{g}. If the RC length for green is an odd number wavelengths of the 532 nm frequency double light from RL and the beatnote frequency is set for an even number of wavelengths, then ν_{PC} will not be resonant with the RC length. Like the optical system for HET, this tuning will be optimized with the shutter open, by maximizing the power of the PC transmitted light that couples to the RC.

In Figure 4 we can see that, like the optical system for the HET, the PLL between RL and the light transmitted by the PC is used to control its length by feeding back to a piezo-electric actuator at the curved mirror. Other than the differences discussed in this section, the optical system for the TES adheres to the same requirements and uses the same methods as those that are used for the HET optical system and discussed in Sections 3.1.1 and 3.1.2.

3.2. Maintaining Spatial Coupling

Another effect which could lead to a loss in sensitivity is related to the alignment of the axion field into the RC. Any difference in the angular alignment or transversal position between the incoming axion field and the optical axis of the cavity eigenmode will reduce the coupling of the axion field to the cavity and lead to a decrease in the regenerated photon rate. To be clear, this will not lead to any misalignment between the detection system and the resonant spatial part of the reconverted field that is amplified in the RC, as its spatial mode will be in the eigenmode of the RC, which is itself aligned to the detectors.

The spatial mode of the axion field entering the RC is an extension of the spatial mode of the field inside the PC and the loss in coupling due to small alignment errors can be calculated from the following equation:

$$1 - \eta_{\mathrm{TM}} \approx \left(\frac{\Delta x}{w_0}\right)^2 + \left(\frac{\Delta\theta}{\theta_{\mathrm{Div}}}\right)^2 \tag{13}$$

where Δx is the transversal shift and $\Delta\theta$ is the angular misalignment between the two modes measured at the waist of the RC [60, 61]. The power loss is quadratic in both terms and required to be less than 5% in total. With a waist size of $w_0 = 6\,\mathrm{mm}$, our requirements of $\Delta x < 1.2\,\mathrm{mm}$ correspond to a loss in the mode matching of 4% due to transversal shifts. Since the divergence angle of the cavities is $\theta_{\mathrm{Div}} = 57\,\mu\mathrm{rad}$, the requirements of $\Delta\theta < 5.7\,\mu\mathrm{rad}$ are equivalent to a 1% loss in the mode matching. The systems that will control the alignment of the cavity mirrors are discussed in the following sections.

3.2.1. Central Mirror Alignment

As the left side of Figure 5 shows, due to the geometry of the cavities, the angular misalignment between their eigenmodes will be equal to the relative misalignment of the flat mirrors at the center of the experiment. Therefore the alignment of these mirrors must be maintained to better than 5.7 µrad to meet our requirements. To accomplish this, both mirrors are mounted to the central optical bench (COB), which is effectively a large stable surface designed for this purpose. It uses no active alignment system and the system instead relies on its passive stability. A system for monitoring the relative alignment drift between the mirrors on the COB for the HET optical system is detailed in [1], but not shown in Figure 5.

The COB is constructed from a single aluminum plate on which all mirrors, beam splitters, and waveplates, as well as position sensors are either mounted directly or through additional ULE base plates [1] using ultra-stable optical mounts. Tests with an autocollimator have shown that a prototype COB was capable of maintaining a long term alignment stability of 2 µrad over one week in air with measured thermal alignment coefficients of $\approx 4\,\mu\mathrm{rad/K}$ in pitch and $\approx 1\,\mu\mathrm{rad/K}$ in yaw [62, 63]. The air conditioning system of the cleanroom has been designed to maintain an 0.1 K absolute temperature stability which would, in principle, eliminate any relevant misalignment. However, the impact of the heating of mirror PC_2 by the cavity internal field on the alignment still needs to be evaluated during the commissioning of the experiment.

3.2.2. End Mirror Alignment

Transversal shifts in the relative positions of the eigenmodes will be determined by the relative alignment of the curved mirrors with respect to the flat mirrors on the COB, ($\Delta\theta_{\mathrm{M}}$). In this case,

the coupling is determined by the ROC of the curved mirrors, R.

$$\Delta x = R\Delta\theta_{\text{M}} \tag{14}$$

We should note here that $\Delta\theta_{\text{M}}$ is not the same as the misalignment given by the cavity eigenmodes $\Delta\theta$. With a radius of curvature in the curved mirrors of 214 m, the relative alignment between the curved and flat mirrors for each cavity must be stabilized to better than 5.6 µrad to meet our requirements of $\Delta x < 1.2$ mm. As we can see, this is quite similar to the requirements on the alignment of the flat mirrors on the COB.

As Figure 5 shows, this is done using two in-vacuum QPDs housed on the COB to monitor the position of the cavity eigenmodes by performing DC differential measurements of the light incident on their quandrants. These QPDs are optimized to sense the position of the 6 mm radius beam with sub 100 µm precision [63]. Assuming that the components on the COB remain stationary, the positions of the eigenmodes on the flat cavity mirrors PC_2 and RC_1, and in extension on the two QPDs, only depend on the orientations of the curved cavity mirrors PC_1 and RC_2, respectively. The differential signals from the QPDs will be fed back to active alignment stages that are capable of controlling the pitch and yaw of the curved cavity end mirrors.

As we will see in the next section, due to the presence of wedge angles in the optics in between the cavities mirrors on the COB, the eigenmodes will have some static transversal shift between them. Nevertheless, this is expected to be below 200 µm. When including the < 3 µrad offsets in the COB cavity mirrors the cumulative mode matching losses due to the static misalignments should be:

$$1 - \eta_{\text{TM}} \approx \left(\frac{\Delta x}{w_0}\right)^2 + \left(\frac{\Delta\theta}{\theta_{\text{Div}}}\right)^2 < 0.5\%. \tag{15}$$

This is on the same order as the matching between the axion field and the PC transmitted field after traversing the COB optics, leaving significant margin for systematic errors and drifts.

3.2.3. Quantifying the transversal matching

Like the tuning of PLL offset frequency, the alignment of the cavity eigenmodes will be quantified using the PC transmitted field when the shutter is open. This quantification has a systematic error due to the refraction of the beams that pass through the optical components located between the cavity internal fields. The substrates of the cavity end mirrors have known wedge angles θ_{W} between 3 and 4 µrad which will refract the PC transmitted field, but not the axion field. By clocking the two substrates correctly to minimize their differential wedge angle $\Delta\theta_{\text{W}}$, the refraction angles will compensate each other such that the final angular refraction is:

$$\theta_{\text{refr}} = (n-1)\Delta\theta_{\text{W}} < 1\,\mu\text{rad} \tag{16}$$

The refraction in PC_2 will laterally shift the PC transmitted beam by $\Delta x < 4\,\mu m$, well below the level of the other sources of alignment noise.

The optics in between the cavity mirrors are also made from substrates with known wedge angles between 2 and 5 µrad and will also be clocked to reduce the overall deflection to below 2 µrad. The total deflection angle between the beams will therefore be below 3 µrad.

Each substrate in between the cavity mirrors will laterally shift the beam off of the optical axis of the system by:

$$y = d\frac{\sin(\theta_1 - \theta_2)}{\cos\theta_2} \qquad \sin\theta_1 = n\sin\theta_2 \tag{17}$$

where d is the thickness of the substrate, θ_1 the angle of incidence, θ_2 the angle inside the material, and n the index of refraction. To cancel the cumulative effect, the number of substrates which shift the beam to the left has to be equal to the number of substrates which shift the beam to the right, assuming that the substrates are equal in thickness and in material, and that the angle of incidence is the same. The COB design [1] uses two substrates that shift the beam left and two that shift it right; all at 35° angle of incidence and all made from fused silica. According to the vendor, the substrates are 9.5 mm thick with a tolerance of $[+0, -0.5\,\text{mm}]$. This results in a worst case lateral shift of $\sim 200\,\mu m$.

Based on these numbers, the uncertainty in the resulting mode mismatch between the PC transmitted field and the axion field for both degrees of freedom will be below 0.4% which will allow us to use the PC transmitted field to verify that the overall alignment of the axion mode into the RC is better than 95%.

4. Summary and Conclusion

ALPS II is designed to be the most sensitive LSW experiment to date with a regenerated photon rate more than 12 orders of magnitude larger than previous experiments. The innovations in the optical system alone account for more than 6 orders of magnitude of the increase in the regenerated signal while the additional boost will come from the long magnetic field length and improvements in detector technologies [45, 48, 1]. Two 122 m, high-finesse optical cavities are largely responsible for the gains from optical system. The use of these cavities, however, presents a unique set of challenges related to maintaining their coherence and spatial overlap. In this paper we have described the core components of ALPS II, and how the optical system is designed to address these challenges.

We will take great care that the spatial mode of the transmitted light from the PC that is incident on the RC is an accurate representation of the axion mode. This will allow us to quantify the coherence and mode matching of the axion field with respect to the RC. The length and alignment sensing system for the lasers and the cavities is based on PDH and DWS, well established phase

sensing schemes with sufficient sensitivity to monitor all relevant degrees of freedom. Additionally, we developed and tested different actuators which should have enough range and bandwidth to operate ALPS II in the HERA tunnels.

We also discussed our plans to employ two different schemes to detect the regenerated photon signal. The first one is the HET and is described in detail in an accompanying paper, while the second scheme uses a TES and will be implemented following the HET science runs. The experiment itself is presently under construction and aiming for a first science run in 2021. Once fully operational, the optical system should allow ALPS II to be able to detect axions with a 95% confidence level for coupling constants as low as $g_{a\gamma\gamma} = 2 \times 10^{-11}/\mathrm{GeV}$ using 20 days of valid science data.

Acknowledgments

The work is supported by the Deutsche Forschungsgemeinschaft [grant number WI 1643/2-1], by the German Volkswagen Stiftung, the National Science Foundation [grant numbers PHY-2110705 and PHY-1802006], the Heising Simons Foundation [grant numbers 2015-154 and 2020-1841], and the UK Science and Technologies Facilities Council [grant number ST/T006331/1].

References

[1] A. Hallal, G. Messineo, M. D. Ortiz, J. Gleason, H. Hollis, D. Tanner, G. Mueller, A. Spector, The heterodyne sensing system for the ALPS II search for sub-ev weakly interacting particles, Physics of the Dark Universe (2021) 100914doi:https://doi.org/10.1016/j.dark.2021.100914.
URL https://www.sciencedirect.com/science/article/pii/S2212686421001382

[2] R. D. Peccei, H. R. Quinn, CP conservation in the presence of pseudoparticles, Phys. Rev. Lett. 38 (25) (1977) 1440.

[3] C. Abel, S. Afach, N. J. Ayres, C. A. Baker, G. Ban, G. Bison, K. Bodek, V. Bondar, M. Burghoff, E. Chanel, Z. Chowdhuri, P.-J. Chiu, B. Clement, C. B. Crawford, M. Daum, S. Emmenegger, L. Ferraris-Bouchez, M. Fertl, P. Flaux, B. Franke, A. Fratangelo, P. Geltenbort, K. Green, W. C. Griffith, M. van der Grinten, Z. D. Grujić, P. G. Harris, L. Hayen, W. Heil, R. Henneck, V. Hélaine, N. Hild, Z. Hodge, M. Horras, P. Iaydjiev, S. N. Ivanov, M. Kasprzak, Y. Kermaidic, K. Kirch, A. Knecht, P. Knowles, H.-C. Koch, P. A. Koss, S. Komposch, A. Kozela, A. Kraft, J. Krempel, M. Kuźniak, B. Lauss, T. Lefort, Y. Lemière, A. Leredde, P. Mohanmurthy, A. Mtchedlishvili, M. Musgrave, O. Naviliat-Cuncic, D. Pais,

F. M. Piegsa, E. Pierre, G. Pignol, C. Plonka-Spehr, P. N. Prashanth, G. Quéméner, M. Rawlik, D. Rebreyend, I. Rienäcker, D. Ries, S. Roccia, G. Rogel, D. Rozpedzik, A. Schnabel, P. Schmidt-Wellenburg, N. Severijns, D. Shiers, R. Tavakoli Dinani, J. A. Thorne, R. Virot, J. Voigt, A. Weis, E. Wursten, G. Wyszynski, J. Zejma, J. Zenner, G. Zsigmond, Measurement of the Permanent Electric Dipole Moment of the Neutron, Phys. Rev. Lett. 124 (2020) 081803. doi:10.1103/PhysRevLett.124.081803.
URL https://link.aps.org/doi/10.1103/PhysRevLett.124.081803

[4] S. Weinberg, A new light boson?, Phys. Rev. Lett. 40 (4) (1978) 223.

[5] F. Wilczek, Problem of Strong P and T Invariance in the Presence of Instantons, Phys. Rev. Lett. 40 (5) (1978) 279.

[6] V. Anastassopoulos, S. Aune, K. Barth, A. Belov, H. Bräuninger, G. Cantatore, J. Carmona, J. Castel, S. Cetin, F. Christensen, et al., New CAST limit on the axion–photon interaction, Nat. Phys. 13 (6) (2017) 584.

[7] K. Ehret, M. Frede, S. Ghazaryan, M. Hildebrandt, E.-A. Knabbe, D. Kracht, A. Lindner, J. List, T. Meier, N. Meyer, et al., New ALPS results on hidden-sector lightweights, Phys. Lett. 689 (4-5) (2010) 149–155.

[8] R. Ballou, G. Deferne, M. Finger Jr, M. Finger, L. Flekova, J. Hosek, S. Kunc, K. Macuchova, K. Meissner, P. Pugnat, et al., New exclusion limits on scalar and pseudoscalar axionlike particles from light shining through a wall, Phys. Rev. D 92 (9) (2015) 092002.

[9] F. Della Valle, E. Milotti, A. Ejlli, G. Messineo, L. Piemontese, G. Zavattini, U. Gastaldi, R. Pengo, G. Ruoso, First results from the new PVLAS apparatus: A new limit on vacuum magnetic birefringence, Phys. Rev. D 90 (2014) 092003. doi:10.1103/PhysRevD.90.092003.
URL https://link.aps.org/doi/10.1103/PhysRevD.90.092003

[10] S. Asztalos, E. Daw, H. Peng, L. J. Rosenberg, C. Hagmann, D. Kinion, W. Stoeffl, K. van Bibber, P. Sikivie, N. S. Sullivan, D. B. Tanner, F. Nezrick, M. S. Turner, D. M. Moltz, J. Powell, M.-O. André, J. Clarke, M. Mück, R. F. Bradley, Large-scale microwave cavity search for dark-matter axions, Phys. Rev. D 64 (2001) 092003. doi:10.1103/PhysRevD.64.092003.
URL https://link.aps.org/doi/10.1103/PhysRevD.64.092003

[11] N. Du, N. Force, R. Khatiwada, E. Lentz, R. Ottens, L. Rosenberg, G. Rybka, G. Carosi, N. Woollett, D. Bowring, et al., Search for invisible axion dark matter with the axion dark matter experiment, Phys. Rev. Lett. 120 (15) (2018) 151301.

[12] T. Braine, R. Cervantes, N. Crisosto, N. Du, S. Kimes, L. J. Rosenberg, G. Rybka, J. Yang, D. Bowring, A. S. Chou, R. Khatiwada, A. Sonnenschein, W. Wester, G. Carosi, N. Woollett, L. D. Duffy, R. Bradley, C. Boutan, M. Jones, B. H. LaRoque, N. S. Oblath, M. S. Taubman, J. Clarke, A. Dove, A. Eddins, S. R. O'Kelley, S. Nawaz, I. Siddiqi, N. Stevenson, A. Agrawal, A. V. Dixit, J. R. Gleason, S. Jois, P. Sikivie, J. A. Solomon, N. S. Sullivan, D. B. Tanner, E. Lentz, E. J. Daw, J. H. Buckley, P. M. Harrington, E. A. Henriksen, K. W. Murch, Extended Search for the Invisible Axion with the Axion Dark Matter Experiment, Phys. Rev. Lett. 124 (2020) 101303. doi:10.1103/PhysRevLett.124.101303.
URL https://link.aps.org/doi/10.1103/PhysRevLett.124.101303

[13] C. Boutan, M. Jones, B. H. LaRoque, N. S. Oblath, R. Cervantes, N. Du, N. Force, S. Kimes, R. Ottens, L. J. Rosenberg, G. Rybka, J. Yang, G. Carosi, N. Woollett, D. Bowring, A. S. Chou, R. Khatiwada, A. Sonnenschein, W. Wester, R. Bradley, E. J. Daw, A. Agrawal, A. V. Dixit, J. Clarke, S. R. O'Kelley, N. Crisosto, J. R. Gleason, S. Jois, P. Sikivie, I. Stern, N. S. Sullivan, D. B. Tanner, P. M. Harrington, E. Lentz, Piezoelectrically Tuned Multimode Cavity Search for Axion Dark Matter, Phys. Rev. Lett. 121 (2018) 261302. doi:10.1103/PhysRevLett.121.261302.
URL https://link.aps.org/doi/10.1103/PhysRevLett.121.261302

[14] S. DePanfilis, A. C. Melissinos, B. E. Moskowitz, J. T. Rogers, Y. K. Semertzidis, W. U. Wuensch, H. J. Halama, A. G. Prodell, W. B. Fowler, F. A. Nezrick, Limits on the abundance and coupling of cosmic axions at $4.5 < m_a < 5.0$ μeV, Phys. Rev. Lett. 59 (1987) 839–842. doi:10.1103/PhysRevLett.59.839.
URL https://link.aps.org/doi/10.1103/PhysRevLett.59.839

[15] W. U. Wuensch, S. De Panfilis-Wuensch, Y. K. Semertzidis, J. T. Rogers, A. C. Melissinos, H. J. Halama, B. E. Moskowitz, A. G. Prodell, W. B. Fowler, F. A. Nezrick, Results of a laboratory search for cosmic axions and other weakly coupled light particles, Phys. Rev. D 40 (1989) 3153–3167. doi:10.1103/PhysRevD.40.3153.
URL https://link.aps.org/doi/10.1103/PhysRevD.40.3153

[16] C. Hagmann, P. Sikivie, N. S. Sullivan, D. B. Tanner, Results from a search for cosmic axions, Phys. Rev. D 42 (1990) 1297–1300. doi:10.1103/PhysRevD.42.1297.
URL https://link.aps.org/doi/10.1103/PhysRevD.42.1297

[17] B. M. Brubaker, L. Zhong, Y. V. Gurevich, S. B. Cahn, S. K. Lamoreaux, M. Simanovskaia, J. R. Root, S. M. Lewis, S. Al Kenany, K. M. Backes, I. Urdinaran, N. M. Rapidis, T. M.

Shokair, K. A. van Bibber, D. A. Palken, M. Malnou, W. F. Kindel, M. A. Anil, K. W. Lehnert, G. Carosi, First Results from a Microwave Cavity Axion Search at 24 μeV, Phys. Rev. Lett. 118 (2017) 061302. doi:10.1103/PhysRevLett.118.061302.
URL https://link.aps.org/doi/10.1103/PhysRevLett.118.061302

[18] L. Zhong, S. Al Kenany, K. M. Backes, B. M. Brubaker, S. B. Cahn, G. Carosi, Y. V. Gurevich, W. F. Kindel, S. K. Lamoreaux, K. W. Lehnert, S. M. Lewis, M. Malnou, R. H. Maruyama, D. A. Palken, N. M. Rapidis, J. R. Root, M. Simanovskaia, T. M. Shokair, D. H. Speller, I. Urdinaran, K. A. van Bibber, Results from phase 1 of the HAYSTAC microwave cavity axion experiment, Phys. Rev. D 97 (2018) 092001. doi:10.1103/PhysRevD.97.092001.
URL https://link.aps.org/doi/10.1103/PhysRevD.97.092001

[19] M. V. Beznogov, E. Rrapaj, D. Page, S. Reddy, Constraints on axion-like particles and nucleon pairing in dense matter from the hot neutron star in HESS J1731-347, Phys. Rev. C 98 (2018) 035802. doi:10.1103/PhysRevC.98.035802.
URL https://link.aps.org/doi/10.1103/PhysRevC.98.035802

[20] M. Meyer, M. Giannotti, A. Mirizzi, J. Conrad, M. A. Sánchez-Conde, Fermi Large Area Telescope as a Galactic Supernovae Axionscope, Phys. Rev. Lett. 118 (2017) 011103. doi:10.1103/PhysRevLett.118.011103.
URL https://link.aps.org/doi/10.1103/PhysRevLett.118.011103

[21] D. Grin, G. Covone, J.-P. Kneib, M. Kamionkowski, A. Blain, E. Jullo, Telescope search for decaying relic axions, Phys. Rev. D 75 (2007) 105018. doi:10.1103/PhysRevD.75.105018.
URL https://link.aps.org/doi/10.1103/PhysRevD.75.105018

[22] J. E. Kim, Weak-Interaction Singlet and Strong CP Invariance, Phys. Rev. Lett. 43 (1979) 103–107. doi:10.1103/PhysRevLett.43.103.
URL https://link.aps.org/doi/10.1103/PhysRevLett.43.103

[23] M. Shifman, A. Vainshtein, V. Zakharov, Can confinement ensure natural CP invariance of strong interactions?, Nuclear Physics B 166 (3) (1980) 493 – 506. doi:https://doi.org/10.1016/0550-3213(80)90209-6.
URL http://www.sciencedirect.com/science/article/pii/0550321380902096

[24] M. Dine, W. Fischler, M. Srednicki, A simple solution to the strong CP problem with a harmless axion, Physics Letters B 104 (3) (1981) 199 – 202. doi:https://doi.org/10.1016/0370-2693(81)90590-6.
URL http://www.sciencedirect.com/science/article/pii/0370269381905906

[25] A. Zhitnitsky, Sov. J. Nucl. Phys. 31 (1980).

[26] S. L. Cheng, C. Q. Geng, W.-T. Ni, Axion-photon couplings in invisible axion models, Phys. Rev. D 52 (1995) 3132–3135. doi:10.1103/PhysRevD.52.3132.
URL https://link.aps.org/doi/10.1103/PhysRevD.52.3132

[27] M. Meyer, D. Horns, M. Raue, First lower limits on the photon-axion-like particle coupling from very high energy gamma-ray observations, Phys. Rev. D 87 (3) (2013) 035027.

[28] M. Giannotti, I. Irastorza, J. Redondo, A. Ringwald, Cool WISPs for stellar cooling excesses, J. Cosmol. Astropart. P. 2016 (05) (2016) 057.

[29] L. Abbott, P. Sikivie, A cosmological bound on the invisible axion, Physics Letters B 120 (1) (1983) 133 – 136. doi:https://doi.org/10.1016/0370-2693(83)90638-X.
URL http://www.sciencedirect.com/science/article/pii/037026938390638X

[30] M. Dine, W. Fischler, The Not So Harmless Axion, Phys. Lett. B 120 (1983) 137–141. doi:10.1016/0370-2693(83)90639-1.

[31] J. Preskill, M. B. Wise, F. Wilczek, Cosmology of the invisible axion, Physics Letters B 120 (1) (1983) 127 – 132. doi:https://doi.org/10.1016/0370-2693(83)90637-8.
URL http://www.sciencedirect.com/science/article/pii/0370269383906378

[32] J. Ipser, P. Sikivie, Can Galactic Halos Be Made of Axions?, Phys. Rev. Lett. 50 (1983) 925–927. doi:10.1103/PhysRevLett.50.925.
URL https://link.aps.org/doi/10.1103/PhysRevLett.50.925

[33] M. Tanabashi, K. Hagiwara, K. Hikasa, K. Nakamura, Y. Sumino, F. Takahashi, J. Tanaka, K. Agashe, G. Aielli, C. Amsler, et al., Review of particle physics, Phys. Rev. D 98 (3) (2018) 030001.

[34] P. Sikivie, Experimental Tests of the "Invisible" Axion, Phys. Rev. Lett. 51 (1983) 1415–1417. doi:10.1103/PhysRevLett.51.1415.
URL https://link.aps.org/doi/10.1103/PhysRevLett.51.1415

[35] P. Brun, A. Caldwell, L. Chevalier, G. Dvali, P. Freire, E. Garutti, S. Heyminck, J. Jochum, S. Knirck, M. Kramer, et al., A new experimental approach to probe QCD axion dark matter in the mass range above 40 μeV, Eur. Phys. J. C 79 (3) (2019) 1–16.

[36] E. Armengaud, F. Avignone, M. Betz, P. Brax, P. Brun, G. Cantatore, J. Carmona, G. Carosi, F. Caspers, S. Caspi, et al., Conceptual design of the international axion observatory (IAXO), J. Instrum. 9 (05) (2014) T05002.

[37] K. Van Bibber, N. Dagdeviren, S. Koonin, A. Kerman, H. Nelson, Proposed experiment to produce and detect light pseudoscalars, Phys. Rev. Lett. 59 (7) (1987) 759.

[38] R. Bähre, B. Döbrich, J. Dreyling-Eschweiler, S. Ghazaryan, R. Hodajerdi, D. Horns, F. Januschek, E.-A. Knabbe, A. Lindner, D. Notz, et al., Any light particle search II—technical design report, J. Instrum. 8 (09) (2013) T09001.

[39] P. Sikivie, D. Tanner, K. van Bibber, Resonantly enhanced axion-photon regeneration, Phys. Rev. Lett. 98 (17) (2007) 172002.

[40] J. Redondo, A. Ringwald, Light shining through walls, Contemp. Phys. 52 (3) (2011) 211–236.

[41] F. Hoogeveen, T. Ziegenhagen, Production and detection of light bosons using optical resonators, Nucl. Phys. 358 (1) (1991) 3–26.

[42] Y. Fukuda, T. Kohmoto, S. I. Nakajima, M. Kunitomo, Production and detection of axions by using optical resonators, Prog. Cryst. Growth Ch. 33 (1-3) (1996) 363–366.

[43] H. Gies, J. Jaeckel, A. Ringwald, Polarized light propagating in a magnetic field as a probe for millicharged fermions, Phys. Rev. Lett. 97 (14) (2006) 140402.

[44] J. H. Põld, H. Grote, ALPS II design requirements document (2019).

[45] C. Albrecht, S. Barbanotti, H. Hintz, K. Jensch, R. Klos, W. Maschmann, O. Sawlanski, M. Stolper, D. Trines, Straightening of superconducting HERA dipoles for the any-light-particle-search experiment ALPS II, EPJ Techniques and Instrumentation 8 (1) (2021) 5.

[46] P. Arias, J. Jaeckel, J. Redondo, A. Ringwald, Optimizing light-shining-through-a-wall experiments for axion and other weakly interacting slim particle searches, Phys. Rev. D 82 (11) (2010) 115018.

[47] Z. R. Bush, S. Barke, H. Hollis, A. D. Spector, A. Hallal, G. Messineo, D. Tanner, G. Mueller, Coherent detection of ultraweak electromagnetic fields, Phys. Rev. D 99 (2) (2019) 022001.

[48] J. Dreyling-Eschweiler, N. Bastidon, B. Döbrich, D. Horns, F. Januschek, A. Lindner, Characterization, 1064 nm photon signals and background events of a tungsten TES detector for the ALPS experiment, J. Mod. Optic. 62 (14) (2015) 1132–1140.

[49] T. J. Kane, R. L. Byer, Monolithic, unidirectional single-mode Nd:YAG ring laser, Opt. Lett. 10 (2) (2007) 65–67.

[50] M. Frede, B. Schulz, R. Wilhelm, P. Kwee, F. Seifert, B. Willke, D. Kracht, Fundamental mode, single-frequency laser amplifier for gravitational wave detectors, Opt. Express 15 (2) (2007) 459–465.

[51] R. Drever, J. L. Hall, F. Kowalski, J. Hough, G. Ford, A. Munley, H. Ward, Laser phase and frequency stabilization using an optical resonator, Appl. Phys. B 31 (2) (1983) 97–105.

[52] E. D. Black, An introduction to Pound–Drever–Hall laser frequency stabilization, Am. J. Phys. 69 (1) (2001) 79–87.

[53] E. Morrison, B. J. Meers, D. I. Robertson, H. Ward, Automatic alignment of optical interferometers, Appl. Opt. 33 (22) (1994) 5041–5049.

[54] A. Buikema, C. Cahillane, G. Mansell, C. Blair, R. Abbott, C. Adams, R. Adhikari, A. Ananyeva, S. Appert, K. Arai, et al., Sensitivity and performance of the Advanced LIGO detectors in the third observing run, Phys. Rev. D 102 (6) (2020) 062003.

[55] L. Glover, M. Goff, J. Patel, I. Pinto, M. Principe, T. Sadecki, R. Savage, E. Villarama, E. Arriaga, E. Barragan, et al., Optical scattering measurements and implications on thermal noise in gravitational wave detectors test-mass coatings, Phys. Lett. 382 (33) (2018) 2259–2264.

[56] W. Winkler, K. Danzmann, A. Rüdiger, R. Schilling, Heating by optical absorption and the performance of interferometric gravitational-wave detectors, Phys. Rev. A 44 (11) (1991) 7022.

[57] P. Kwee, C. Bogan, K. Danzmann, M. Frede, H. Kim, P. King, J. H. Põld, O. Puncken, R. L. Savage, F. Seifert, P. Wessels, L. Winkelmann, B. Willke, Stabilized high-power laser system for the gravitational wave detector advanced LIGO, Opt. Express 20 (10) (2012) 10617–10634. doi:10.1364/OE.20.010617.
URL http://www.opticsexpress.org/abstract.cfm?URI=oe-20-10-10617

[58] J. I. Thorpe, K. Numata, J. Livas, Laser frequency stabilization and control through offset sideband locking to optical cavities, Opt. Express 16 (20) (2008) 15980–15990.

[59] J. H. Põld, A. D. Spector, Demonstration of a length control system for ALPS II with a high finesse 9.2 m cavity, Eur. Phys. J. TI 7 (1) (2020) 1–9.

[60] G. Mueller, P. Sikivie, D. Tanner, K. Van Bibber, Detailed design of a resonantly enhanced axion-photon regeneration experiment, Phys. Rev. D 80 (7) (2009) 072004.

[61] G. Mueller, P. Sikivie, D. B. Tanner, K. Van Bibber, Resonantly-enhanced axion-photon regeneration, in: AIP Conference Proceedings, Vol. 1274, American Institute of Physics, 2010, pp. 150–155.

[62] S. Kulkarni, A. Umińska, J. Gleason, S. Barke, R. Ferguson, J. Sanjuán, P. Fulda, G. Mueller, Ultrastable optical components using adjustable commercial mirror mounts anchored in a ULE spacer, Appl. Opt. 59 (23) (2020) 6999–7003.

[63] L.-W. Wei, K. Karan, B. Willke, Optics mounting and alignment for the central optical bench of the dual cavity enhanced light-shining-through-a-wall experiment ALPS II, Appl. Opt. 59 (28) (2020) 8839–8847. doi:10.1364/AO.401346.
URL http://ao.osa.org/abstract.cfm?URI=ao-59-28-8839